Optical conductivity in the *t-J* Holstein model

L. Vidmar,[1] J. Bonča,[2,1] and S. Maekawa[3,4]
[1]*J. Stefan Institute, 1000 Ljubljana, Slovenia*
[2]*Faculty of Mathematics and Physics, University of Ljubljana, 1000 Ljubljana, Slovenia*
[3]*Institute for Materials Research, Tohoku University, Sendai 980-8577, Japan*
[4]*CREST, Japan Science and Technology Agency (JST), Kawaguchi, Saitama 332-0012, Japan*
(Received 30 October 2008; revised manuscript received 17 January 2009; published 30 March 2009)

Using a recently developed numerical method we compute charge stiffness and optical conductivity of the *t-J* model coupled to optical phonons. Coherent hole motion is most strongly influenced by the electron-phonon coupling within the physically relevant regime of the exchange interaction. We find unusual nonmonotonous dependence of the charge stiffness as a function of the exchange coupling near the crossover to the strong electron-phonon coupling regime. Optical conductivity in this regime shows a two-peak structure. The low-frequency peak represents local magnetic excitation, attached to the hole, while the higher-frequency peak corresponds to the mid-infrared band that originates from coupling to spin-wave excitations, broadened and renormalized by phonon excitations. We observe no separate peak at or slightly above the phonon frequency. This finding suggests that in the framework of the *t-J* Holstein model the two-peak structure seen in recent optical measurements is due to magnetic excitations coupled to lattice degrees of freedom via doped charge carriers.

DOI: 10.1103/PhysRevB.79.125120 PACS number(s): 71.10.Pm, 71.27.+a, 71.38.−k, 78.67.−n

I. INTRODUCTION

Despite many years of intensive research of transport properties of a hole doped in an antiferromagnetic background the proper description of this system remains a challenging theoretical problem. The transport of a doped hole leaves in its wake locally distorted, slowly relaxing spin background, leading to the formation of a dressed quasiparticle with an enhanced effective mass and renormalized charge stiffness—a measure of a coherent, free-particle-like transport. Addition of lattice degrees of freedom to this already elaborate problem reflects the current scientific interest in the field of correlated electron systems.

Long after the pioneering work,[1] the enhanced interest in correlated models, coupled to lattice degrees of freedom is primarily fueled by experimental evidence given in part by angular resolved photoemission data demonstrating that strong electron-phonon (EP) interaction plays an important role in low-energy physics of high-T_c materials.[2–5] Moreover, recent estimates of transport based on the pure *t-J* model[6] yield substantially smaller resistivity in comparison to experiments in the low-doping regime of $La_{2-x}Sr_xCuO_4$, that can be explained as a lack of additional lattice degrees of freedom.

Recent numerical methods investigating optical conductivity (OC) in correlated electron systems and systems, where electrons are coupled to bosonic degrees of freedom, have been focused on the generalized *t-J* model,[7,8] Holstein and generalized electron-boson model,[9,10] while investigations of the *t-J* Holstein model have been until recently limited to small clusters with ten sites.[11] Diagrammatic quantum Monte Carlo (DMC) method has been applied to resolve OC of the Fröhlich polaron[12] and recently also the *t-J* Holstein model.[13] In the later work authors report on a two-peak structure in the optical response where the low-ω peak is due to polaronic effects while the peak at higher ω is due to magnetic excitations, renormalized by lattice degrees of freedom. DMC method does not reproduce the well known string states seen in the spectral function[14] neither the signature of local magnetic excitations in optical conductivity since authors use the self-consistent Born approximation (SCBA) without magnon-magnon vertex corrections for treating spin degrees of freedom. Their result seems to contradict calculations based on the dynamical mean-field theory (DMFT) where a two-peak structure is seen in OC only at small $J/t \lesssim 0.3$.[15] In this work authors also show that the low-ω peak is of the magnetic origin while the higher-ω peak represents the broad polaronic band.

II. MODEL AND NUMERICAL METHOD

The main goal of this work is to investigate in depth optical properties of the *t-J* Holstein model for the case of a single hole in the antiferromagnetic background. We first define the *t-J* Holstein model on a square lattice

$$H = -t\sum_{\langle i,j\rangle,s} \tilde{c}^{\dagger}_{i,s}\tilde{c}_{j,s} + J\sum_{\langle i,j\rangle} \mathbf{S}_i\mathbf{S}_j + g\sum_i (1-n_i)(a_i^+ + a_i) + \omega_0\sum_i a_i^+ a_i, \quad (1)$$

where $\tilde{c}_{i,s}=c_{i,s}(1-n_{i,-s})$ is a fermion operator, projected onto a space of no double occupancy, t represents nearest-neighbor overlap integral, the sum $\langle i,j\rangle$ runs over pairs of nearest neighbors, a_i are phonon annihilation operators, and $n_i=\Sigma_s n_{i,s}$. The third term represents EP coupling $g=\sqrt{8\lambda\omega_0 t}$, where λ is the dimensionless EP coupling constant, and the last term represents the energy of Einstein phonons ω_0.

We use a recently developed method based on the exact diagonalization within the limited functional space (EDLFS).[16,17] Since details of the method have been published elsewhere,[16–18] we now briefly discuss only the main

steps of the method. We first construct the limited functional space by starting from a Néel state with one hole with a given momentum $\mathbf{k}$ and zero phonon degrees of freedom $|\phi_{\mathbf{k}}^{(0,0)}\rangle = c_{\mathbf{k}}|\text{Neel};0\rangle$, and applying the generator of states $\{|\phi_{\mathbf{k}l}^{(N_h,M)}\rangle\} = (H_{\text{kin}}+H_g^M)^{N_h}|\phi_{\mathbf{k}}^{(0,0)}\rangle$, where H_{kin} and H_g represent the first and the third terms, respectively, of Eq. (1). This procedure generates exponentially growing basis space of states, consisting of different shapes of strings in the vicinity of the hole with maximum lengths given by N_h as well as phonon quanta that are as well located in the vicinity of the hole, at a maximal distance N_h. Parameter M provides generation of additional phonon quanta leading to a maximum number $N_{\text{ph}}^{\max} = MN_h$. Full Hamiltonian given by Eq. (1) is diagonalized within this limited functional space taking into account the translational symmetry while the continued fraction expansion is used to obtain dynamical properties of the model. The method treats spin, charge, as well as lattice degrees of freedom, on equal footing.

We define OC per doped hole[19]

$$\boldsymbol{\sigma}(\omega) = \frac{i}{\omega^+}[\langle\boldsymbol{\tau}\rangle - \boldsymbol{\chi}(\omega)], \tag{2}$$

$$\boldsymbol{\chi}(\omega) = i\int_0^\infty e^{i\omega^+ t}\langle[\mathbf{j}(t),\mathbf{j}(0)]\rangle dt, \tag{3}$$

where $\boldsymbol{\tau} = \Sigma_{\langle i,j\rangle,s} t_{ij}(\mathbf{R}_{ij}\otimes\mathbf{R}_{ij})\tilde{c}_{j,s}^\dagger \tilde{c}_{i,s}$ represents the stress tensor, $\mathbf{j} = i\Sigma_{\langle i,j\rangle,s} t_{ij}\mathbf{R}_{ij}\tilde{c}_{j,s}^\dagger \tilde{c}_{i,s}$ is the current operator, $t_{ij} = -t$ for next-nearest neighbors only and zero otherwise, and $\mathbf{R}_{ij} = \mathbf{R}_j - \mathbf{R}_i$. We also note that in the case of next-neighbor tight-binding models, $\langle\boldsymbol{\tau}\rangle$ is related to the kinetic energy, $\langle\tau_{\mu,\mu}\rangle = -\langle H_{\text{kin}}\rangle/2$.

III. CHARGE STIFFNESS AND SUM-RULES

Charge stiffness per doped hole can be on a square lattice for the t-J Holstein model computed via its spectral representation[20]

$$D_{\mu,\mu} = -\frac{1}{4}\langle 0|H_{\text{kin}}|0\rangle + \sum_n \frac{\langle 0|j_\mu|n\rangle\langle n|j_\mu|0\rangle}{(E_0 - E_n)}, \tag{4}$$

$$D_{\mu,\mu} = S^{\text{tot}} - S_{\mu,\mu}^{\text{reg}}, \tag{5}$$

where S^{tot} represents normalized optical sum rule $\int_{-\infty}^{\infty}\sigma'_{\mu,\mu}(\omega)d\omega = 2\pi S^{\text{tot}}$, while S^{reg} is defined by $\int_{0^+}^{\infty}\sigma'_{\mu,\mu}(\omega)d\omega = \pi S_{\mu,\mu}^{\text{reg}}$ and $\boldsymbol{\sigma}'(\omega)$ represents the real part of the optical conductivity tensor in Eq. (2). We have computed $D_{\mu,\mu}$ in the single-hole ground state, i.e., at $\mathbf{k} = (\pm\pi/2, \pm\pi/2)$. It is well known that the dispersion $E(\mathbf{k})$ is highly anisotropic around its single-hole minimum, which is in turn reflected in the anisotropy of the effective mass tensor.[1,8,21] It is thus instructive to compute tensors representing the charge stiffness as well as the OC in the direction of their eigenaxis, i.e., along the nodal $[(\pi/2,\pi/2)\rightarrow(0,0)]$ direction that gives $D_\parallel$, $\sigma_\parallel(\omega)$, and along the antinodal $[(\pi/2,\pi/2)\rightarrow(\pi,0)]$ direction that leads to $D_\perp$, and $\sigma_\perp(\omega)$.

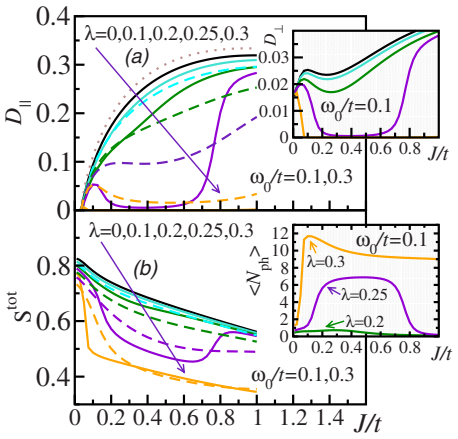

FIG. 1. (Color online) (a) Charge stiffness $D_\parallel$ ($D_\perp$ in the inset), (b) optical sum rule S^{tot} ($\langle N_{\text{ph}}\rangle = \Sigma_i a_i^\dagger a_i$ in the inset vs J/t at $\omega_0/t = 0.1$ (full lines) and $\omega_0/t = 0.3$ (dashed lines). In this and all subsequent figures [except for the dotted line in (a) or else otherwise indicated] we used: $N_h = 8$, $M = 7$, and $N_{\text{st}} \sim 9\times 10^6$. Dotted line in (a) was for $\lambda = 0$ obtained with states with zero phonon degrees of freedom and the following set of parameters: $N_h = 14$, $M = 0$, and $N_{\text{st}} \sim 5\times 10^6$.

In Fig. 1(a) we present the charge stiffness vs J/t for various values of EP coupling strength. To obtain accurate results in the strong EP coupling (SC) limit, we had to rely on only $N_{\text{st}} = 9786$ different combinations of spin-flip states, while the total number of states, including phonon degrees of freedom, was $N_{\text{st}} = 9\times 10^6$. To test the quality of $\lambda = 0$ results, we show with the dashed line $D_\parallel$ computed with zero phonon degrees of freedom using $N_{\text{st}} = 5\times 10^6$. Agreement with the $\lambda = 0$ case, obtained with $N_{\text{st}} = 9786$ is rather surprising, given the fact that results were computed using Hilbert spaces that differ by nearly three orders of magnitude. This fast convergence is in contrast to calculations on finite-size clusters where due to the existence of persistent currents D varies rather uncontrollably between different system sizes.[22] Nevertheless, our values of D qualitatively agree with results obtained using slave-fermion Schwinger-boson formalism.[23]

Exploring further $\lambda = 0$ results we observe $D_\parallel \sim 0$ at $J/t \sim 0$ indicating strong scattering on spin degrees of freedom. With increasing J/t $D_\parallel$ steeply increases and around $J/t \sim 1$ reaches at $D_\parallel \sim 0.3$ a broad maximum that as well coincides with the maximum of the bandwidth W.[17] In contrast, the optical sum rule $S^{\text{tot}} = -\langle H_{\text{kin}}\rangle/4$ monotonically decreases in the range $0 \lesssim J/t \lesssim 1.0$ with increasing J/t, Fig. 1(b). Due to strong anisotropy in $E(\mathbf{k})$, $D_\perp$ remains nearly an order of magnitude smaller than $D_\parallel$ for $J/t \gtrsim 0.2$ [see the inset of Fig. 1(a)].

Turning to finite λ, $D_\parallel$ expectedly decreases, due to additional scattering on lattice degrees of freedom. The effect of λ on the value of $D_\parallel$ however varies with J/t. This is best seen in the case of $\lambda = 0.25$ and $\omega_0/t = 0.1$ where $D_\parallel$ is approximately equal to its $\lambda = 0$ value for $J/t \lesssim 0.1$, it then decreases with increasing J/t, reaching its minimum value around $J/t \sim 0.5$ and finally, for larger values of $J/t \gtrsim 0.8$, steeply increases. This nonmonotonous behavior is as well reflected in the bell-shaped average phonon number $\langle N_{\text{ph}}\rangle$ vs J/t, presented in the inset of Fig. 1(b). This behavior is also

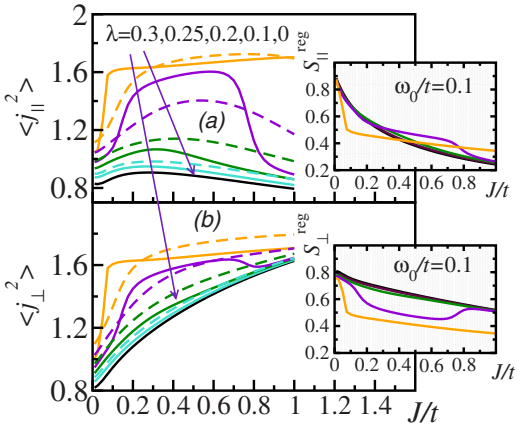

FIG. 2. (Color online) (a) Expectation value of the square of the electrical current along the nodal direction $\langle j_{\parallel}^2\rangle$ ($S_{\parallel}^{\mathrm{reg}}$ in the inset), (b) expectation value of the square of the electrical current along the antinodal direction $\langle j_{\perp}^2\rangle$ ($S_{\perp}^{\mathrm{reg}}$ in the inset) vs J/t at $\omega_0/t=0.1$ (full lines) and $\omega_0/t=0.3$ (dashed lines).

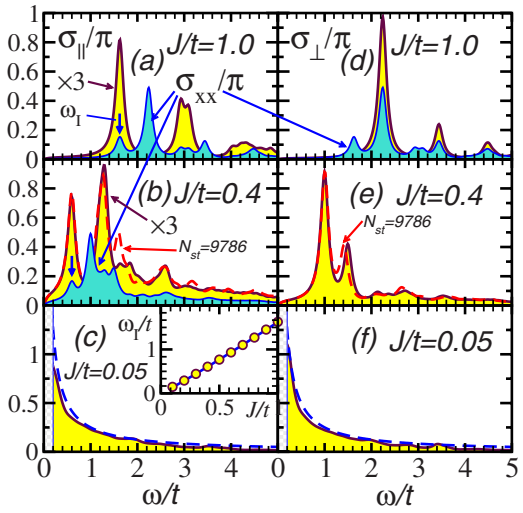

FIG. 3. (Color online) $\sigma_{\parallel}$ in (a)–(c), and $\sigma_{\perp}$ in (d)–(f) for three different values of J/t as indicated in the figures for the *t-J* model for a single doped hole at $\lambda=0$ and $\mathbf{k}=(\pi/2,\pi/2)$. Hilbert space with no phonon degrees of freedom and $N_{\mathrm{st}}=5\times10^6$ was used in all cases except in (b) and (e) where for comparison we in addition present calculations with $N_{\mathrm{st}}=9786$. In (a), (b), and (d) we also show $\sigma_{xx}=(\sigma_{\parallel}+\sigma_{\perp})/2$ using turquoise (dark gray) fill. Arrows in (a) and (b) indicate positions of lowest-energy peaks, ω_{I}. Dashed lines in (c) and (f) are given by $\sigma_{\mu,\mu}(\omega)=\pi/(z\omega)$. Inset in (c) represents scaling of ω_{I} (open circles) vs J/t. In this and in the subsequent figures, the Drude peak is not shown. Artificial broadening $\epsilon=0.1t$ was used. Dashed areas in (c) and (f) delineate small frequency regimes ($\omega/t\lesssim0.2$) where at $J/t=0.05$ EDLFS does not lead accurate results due to the vicinity of the Nagoka regime.

consistent with the nonmonotonous functional dependence of $\lambda_c(J/t)$, representing the crossover EP coupling strength to the SC regime (Refs. 16 and 24).

We now make some general comments about the effect of the EP interaction on the correlated system at the onset of the SC regime. At small values of $J/t\lesssim0.1$ EP coupling is less effective, which seems to be in contrast to naive expectations. We attribute this *disentanglement* from lattice degrees of freedom to the increase in the kinetic energy and the vicinity of the Nagaoka regime. This effect is particularly evident from the J/t dependence of the average phonon number $\langle N_{\mathrm{ph}}\rangle$ at $\lambda=0.3$ [see the inset of Fig. 1(b)] where an increase followed by a sharp drop of $\langle N_{\mathrm{ph}}\rangle$ is seen with lowering of J/t. At the onset of the SC regime, i.e., at $\lambda\sim0.25$, EP coupling is most effective in the physically relevant $J/t\sim0.3-0.4$ regime, where there is a strong competition between kinetic energy and magnetic excitations. The critical λ_c as well reaches its minimum around $J/t\sim0.3$ as shown in Ref. 16. At larger $J/t\sim1$ EP coupling becomes again less effective due to more coherent quasiparticle motion as reflected in the enhanced charge stiffness, quasiparticle weight, as well as the bandwidth.[16,17]

The optical sum rule S^{tot}, presented in Fig. 1(b), as well decreases with increasing λ. It however remains finite even deep in the SC regime where $D_{\parallel}\sim0$ since S^{tot} includes both coherent as well as incoherent transport. The latter remains finite due to processes, where the hole hops back and forth between neighboring sites while leaving lattice deformation unchanged. Despite charge localization we thus expect nonzero optical response $\sigma(\omega)$ even deep in the SC regime, with its spectral weight shifted toward larger ω and zero contribution at $\omega=0$. Due to localization we also expect OC to be isotropic in the SC regime, i.e., $\sigma_{\parallel}(\omega)\sim\sigma_{\perp}(\omega)$.

In the insets of Fig. 2 we show $S_{\parallel}^{\mathrm{reg}}$ and $S_{\perp}^{\mathrm{reg}}$ representing the integrated regular part of the OC. $S_{\parallel}^{\mathrm{reg}}$ steeply decreases with increasing J/t due to the simultaneous increase in coherent transport, captured by $D_{\parallel}$, as well as due to decrease in S^{tot}, see also Eq. (5). We observe that EP coupling has little effect on $S_{\parallel}^{\mathrm{reg}}$ for $J/t\lesssim0.4$, since its value is rather independent on λ except deep in the SC regime, i.e., at $\lambda=0.3$ in this particular case. Due to small values of $D_{\perp}$ we find $S_{\perp}^{\mathrm{reg}}\sim S^{\mathrm{tot}}$, see Figs. 1 and 2.

In Fig. 2 we present the average of the square of the electrical current defining the following sum rule $\int_{0^+}^{\infty}\omega\sigma'_{\mu,\mu}(\omega)d\omega=\pi\langle j_{\mu,\mu}^2\rangle$ that furthermore represents the fluctuation of the current operator. In the ground state there are no persistent currents that usually appear on finite-size clusters, since our method is defined on an infinite lattice. This furthermore enables more reliable calculation of the charge stiffness. At $\lambda=0$ $\langle j_{\parallel}^2\rangle$ [in Fig. 2(a)] and $\langle j_{\perp}^2\rangle$ [in Fig. 2(b)] display rather distinctive J/t dependence. While $\langle j_{\parallel}^2\rangle$ shows weak nonmonotonous dependence on J/t, $\langle j_{\perp}^2\rangle$ shows a substantial increase. With increasing λ current fluctuations as well increase in both directions. In the SC regime we obtain $\langle j_{\parallel}^2\rangle\sim\langle j_{\perp}^2\rangle$ as a consequence of localization due to lattice degrees of freedom.

IV. DYNAMIC PROPERTIES

Turning to dynamic properties we first establish numerical efficiency of our method by presenting optical properties of the *t-J* model. In Fig. 3 we display different components of the conductivity tensor $\sigma_{\mu,\mu}(\omega)$ in the single-hole minimum $\mathbf{k}=(\pi/2,\pi/2)$, computed using EDLFS. At physically relevant value $J/t=0.4$ we reproduce well known features, characteristic of $\sigma_{xx}(\omega)$: (a) in the regime $1.6J\lesssim\omega\lesssim2t$ we

find peaks forming a rather broad band, appearing within the well known mid-infrared (MIR) frequency regime, separated from the Drude peak (not shown) by a gap of the order of J, and (b) there is a broad featureless tail, extending to large frequencies, $\omega \gtrsim 7t$. MIR peaks for $J/t \gtrsim 0.2$ scale with the exchange coupling $(J/t)^{\eta}$, where $\eta \sim 1$. We stress that such scaling is consistent with local magnetic excitations as well as spin waves. Obtained scaling is however *not* consistent with the string picture where $\eta = 2/3$ (see also Ref. 25). At $J/t=0.4$ as well as at $J/t=1$, the lowest-frequency peak in OC appears at $J/t \sim 1.6$. Location of the lowest-frequency peak [indicated by arrows in Figs. 3(a) and 3(b)] is surprisingly close to the location of the peak in OC of the t-J_z model in the limit $J_z/t \to \infty$, given by $\sigma(\omega) \sim t^2/J_z \delta(\omega - \frac{3}{2}J_z)$.[26] In this trivial case the peak appears at the frequency that corresponds to the energy (measured from the Néel state) of a single spin flip, attached to the hole, created as the hole hops one lattice site from its origin in the undisturbed Néel background. It is somewhat surprising that such a naive interpretation seems to survive even in the (spin) isotropic t-J model and at rather small value of $J/t=0.4$. The scaling of the position of the low-frequency peak closely follows the following expression $\omega_I = 1.62(J/t)^{1.08}$, indicated by a dashed line, connecting the circles shown in the inset of Fig. 3(c). Our results of OC qualitatively agree with those, obtained on small lattice systems.[26]

When conductivity tensor $\boldsymbol{\sigma}(\omega)$ is computed in its eigendirections, distinct (incoherent) finite-ω peaks are obtained in the case of $\sigma_{\parallel}(\omega)$ and $\sigma_{\perp}(\omega)$, as best seen at $J/t=1$ and $J/t=0.4$. For comparison we present in Figs. 3(a), 3(b), and 3(d) $\sigma_{xx}(\omega)$ that consists of all the peaks characteristic for both $\sigma_{\parallel}(\omega)$ as well as $\sigma_{\perp}(\omega)$. The reason is, that the ground state at $\mathbf{k}=(\pi/2,\pi/2)$ or Σ point belongs to an irreducible representation Σ_1 of the small group of $\mathbf{k}$, i.e., C_2. Current operators $j_{\parallel}$ and $j_{\perp}$, defining $\sigma_{\parallel}(\omega)$ and $\sigma_{\perp}(\omega)$ through Eqs. (2) and (3) transform as distinct irreducible representations Σ_1 and Σ_2. Selection rules allow only transitions into states that transform according to a direct product of irreducible representations of the group C_2. Since j_x does not transform according to irreducible representations of C_2, the above mentioned selection rules do not apply.

In Figs. 3(b) and 3(e) we present as well results, computed on a much smaller set of states, i.e., with $N_{\mathrm{st}}=9786$. Apart for a small shift of one of the MIR peaks at larger ω, the agreement with results, obtained with more than 3 orders of magnitude larger systems ($N_{\mathrm{st}}=5\times10^6$) underlines the efficiency of our method. Obtaining relevant results for the pure t-J model at moderate number of states is of crucial importance for successful implementation of additional lattice degrees of freedom. Last, we present in Figs. 3(c) and 3(f) results at small $J/t=0.05$. Dashed lines represent known analytical estimate $\sigma(\omega)=\pi/(z\omega)$, where $z=4$ (Ref. 27). This result is characteristic for systems with a nearly constant density of states and diffusive hole motion where current matrix elements $|\langle 0|j_{\mu}|n\rangle|$ are roughly independent of n.[27] Good agreement with the analytical results in the small J/t limit is of particular importance since our method is by construction, based on the existence of the long-range Néel order, targeted to be valid predominantly in the regime of intermediate to large values of the exchange constant J/t. We also note that in the limit of small-J/t optical properties for $\omega/t \gtrsim J/t$ become isotropic.

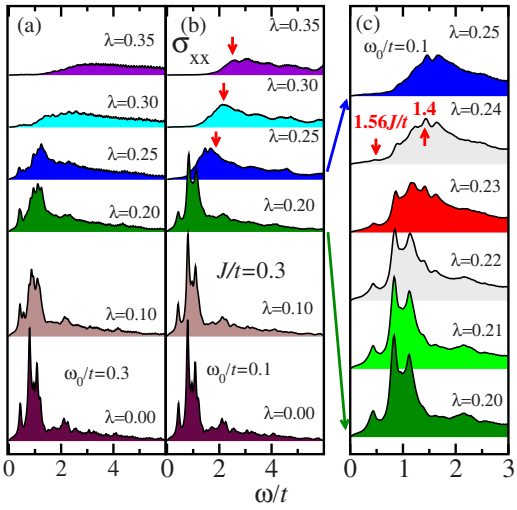

FIG. 4. (Color online) σ_{xx} for $\omega_0/t=0.3$ in (a), $\omega_0/t=0.1$ in (b) and (c) at $J/t=0.3$, and at $\mathbf{k}=(\pi/2,\pi/2)$. Total number of functions was $N_{\mathrm{st}}=9\times10^6$. Up to 56 phonon quanta were used to obtain accurate results for $\lambda \gtrsim 0.2$. Arrows in (b) indicate $\omega_{\mathrm{II}}=16\lambda\tilde{t}$ where $\tilde{t}=0.45t$. Units of σ are arbitrary, yet chosen identical in (a) and (b); a different scale was used for (c), nevertheless identical among different plots in (c). Artificial broadening was set to $\epsilon/t=0.05$.

We now focus on the influence of increasing EP coupling λ on optical properties of the t-J Holstein model in the adiabatic regime, i.e., for $\omega_0/t=0.3$, Fig. 4(a) and $\omega_0/t=0.1$, Figs. 4(b) and 4(c) the latter value being relevant for cuprates. Increasing EP coupling λ leads to three main effects: (a) the spectra progressively shift toward higher frequencies while the total spectral weight decreases [see also the inset of Fig. 2(b)]; (b) magnetic excitations that form a band in the MIR regime broaden and diminish with increasing λ; they finally disappear in the SC regime where they are replaced by a broad polaronlike band that clearly originated from the renormalized MIR peaks. The peak of the well formed broad band at $\omega_0/t=0.1$ in the regime $0.25 \lesssim \lambda \lesssim 0.4$ roughly scales with $\omega_{\mathrm{II}} \sim 16\lambda\tilde{t}$ where $\tilde{t}=0.45t$ represents renormalized hopping due to EP interaction. At $\omega_0/t=0.3$ a broader, featureless band is formed, and (c) a large gap opens in the SC regime.

In contrast to numerical results of Ref. 13, we observe no separate peak at or slightly above the phonon frequency. This is more clearly seen in Fig. 4(c) where $\sigma_{xx}(\omega)$ is shown in an expanded frequency range. This result is consistent with DMFT calculations of Refs. 15 and 28. The lack of a peak at $\omega \gtrsim \omega_0$ in OC can be explained in simple terms in the large J_z/t limit of the simplified t-J_z Holstein model. Starting from a hole in the Néel background, the lowest-energy contribution to $\sigma_{xx}(\omega)$ comes from the hop of the hole to the neighboring site. This move generates a single spin flip with the energy $E_1=3J_z/2$ above the ground state. The contribution to OC that would include a single phonon excitation would thus be located at $\omega \gtrsim 3J_z/2+\omega_0$.

Nevertheless, we find quantitative agreement at $\lambda \sim 0.24$ with measurements on $(Eu_{1-x}Ca_x)Ba_2Cu_3O_6$ in the low hole-

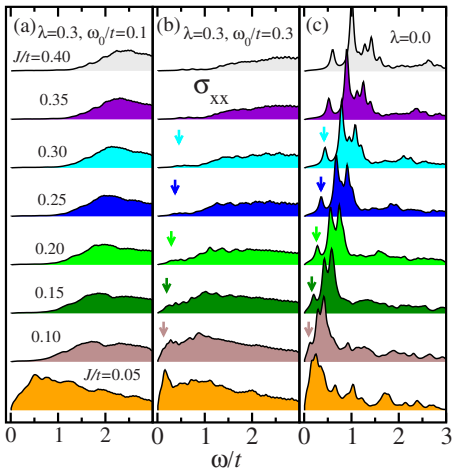

FIG. 5. (Color online) σ_{xx} at $\lambda=0.3$; (a) $\omega_0/t=0.1$, (b) $\omega_0/t=0.3$, and $\lambda=0.0$ in (c) at $\mathbf{k}=(\pi/2,\pi/2)$. Arrows in (b) and (c) indicate positions of the lowest-frequency state as it appears at respective values of J/t at $\lambda=0$. Artificial broadening was set to $\epsilon/t=0.05$.

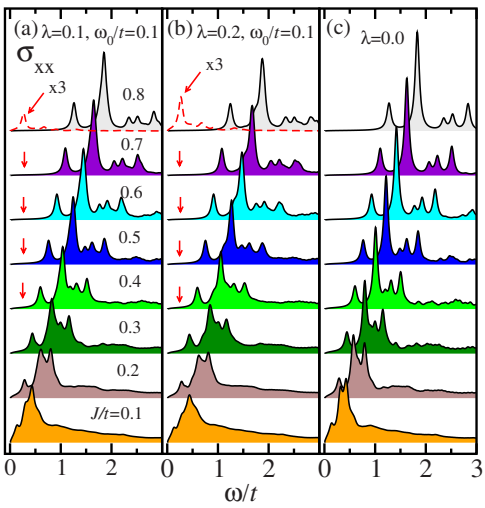

FIG. 6. (Color online) σ_{xx} at $\omega_0/t=0.1$ and $\lambda=0.1$ (a), $\lambda=0.2$ (b), and $\lambda=0.0$ in (c) at $\mathbf{k}=(\pi/2,\pi/2)$ and different values of the exchange interaction J/t as indicated in the figure. Dashed lines, multiplied by a factor of 3 for better visibility, in (a) and (b) (top) represent results of the Holstein model with $\omega_0/t=0.1$, calculated at corresponding values of λ and $\mathbf{k}=(0,0)$. Arrows in (a) and (b) indicate the position of the lowest-ω peak for the Holstein model. In this figure we have used $N_h=12$, $M=1$, and $N_{\mathrm{st}}=27\times10^6$ for the *t-J* Holstein model. Identical parameters N_h and M were used in the case of the Holstein model where due to a lack of spin degrees of freedom $N_{\mathrm{st}}=6\times10^5$. Artificial broadening was set to $\epsilon/t=0.05$.

doping regime published in Ref. 13. In our calculation $\lambda\sim0.24$ represents the maximum EP coupling constant where the low-ω peak, located at $\omega_{\mathrm{I}}\sim1.56J\sim187$ meV (choosing $t=400$ meV and $J/t=0.3$), is just barely visible. This peak is, as discussed above, due to the local magnetic excitation and remains separated from the continuum forming the rest of the MIR band. Experimental value of the corresponding peak is $\omega_{\mathrm{I}}^{\mathrm{exp}}=174$ meV.[13] The higher ω peak at $\omega_{\mathrm{II}}\sim1.4t=560$ meV (experimental value is $\omega_{\mathrm{II}}^{\mathrm{exp}}=590$ meV) corresponds to the MIR band, broadened and renormalized by phonon excitations. This part of OC together with the physical interpretation of the MIR shift due to lattice degrees of freedom is in agreement with calculations in Ref. 13.

Our explanation of the experimental results relies on the conjecture that lightly doped $(Eu_{1-x}Ca_x)Ba_2Cu_3O_6$ compound lies in the crossover from weak to strong coupling electron-phonon regime where physical properties (quasiparticle weight, charge stiffness, and dynamic properties) are extremely sensitive to small changes of λ. This is evident from Fig. 4 and from results published in Ref. 16. The MIR peak in OC is at $\lambda=0$ centered around $\omega_{\mathrm{II}}=2J=240$ meV. This value corresponds to the peak of the magnon density of states;[14] it however underestimates the position of the main peak, seen in the experiment of Ref. 13. With increasing λ beyond the weak coupling regime $\lambda>\lambda_c$, the center of the MIR peaks starts moving toward higher frequencies and broadens as it transforms into a wide polaron band, thus approaching the experimental value. Simultaneously the peak due to the local magnetic excitation at ω_{I} as well broadens and disappears above $\lambda\gtrsim0.24$.

In order to explore the interplay of magnetic and lattice degrees of freedom in the structure of $\sigma_{xx}(\omega)$ in more detail, we present in Figs. 5(a) and 5(b) comparison of optical spectra at fixed $\lambda=0.3$ and different values of the exchange interaction J/t. Decreasing J/t leads to a shift of the broad polaronic peak toward smaller values of ω. At smaller $\omega_0/t=0.1$ more pronounced structure abruptly appears at low $\omega/t\lesssim0.5$ at small $J/t=0.05$, Fig. 5(a). At larger value of $\omega_0/t=0.3$ [Fig. 5(b)] a shoulder starts appearing at $J/t=0.3$ in the low-ω regime that corresponds to the onset of the respective magnetic peaks [as indicated by arrows in Fig. 5(c)] of the pure *t-J* model. Below $J/t\lesssim0.2$ well formed peaks emerge being clearly of the magnetic origin. The disentanglement of lattice degrees of freedom, clearly seen in Fig. 5(b), is consistent with DMFT calculations.[15]

The lack of low-frequency peak above $\omega=\omega_0$ associated with phonon excitations in the limit of weak EP coupling is investigated in Fig. 6. We have applied the EDLFS method to solve the Holstein model with a single electron using essentially identical Hibert space describing lattice degrees of freedom as the one used for the *t-J* Holstein model. $\sigma_{xx}(\omega)$ is for this case presented with dashed lines in Figs. 6(a) and 6(b) for $\lambda=0.1$ and 0.2, respectively. In both cases we observe peaks located near $\omega\sim2.6\omega_0$ with their spectral weights expectedly increasing with increasing λ. In the weak EP coupling limit the size of the excited lattice polaron state, generated by the current operator, acting on the polaron ground state extends beyond the maximal distance l_{max} between the hole and the phonon excitation described within the limited functional space. Even though l_{max} is in our calculation limited to $l_{\mathrm{max}}=N_h-1=11$ lattice sites, it is nevertheless much larger than in typical exact-diagonalization approaches to the *t-J* Holstein model in two dimensions where $l_{\mathrm{max}}=2\sqrt{2}$ (Ref. 11). A simple analytical estimate can be derived in the $\lambda\to0$ limit that predicts the onset of optical spectra due to a finite value of l_{max} at $\omega/t=\omega_0/t+4[1-\cos\pi/(l_{\mathrm{max}}+1)]\sim0.24$ for $\omega_0/t=0.1$ which is in close agreement with the numerical calculations in Fig. 6. The main result of Figs. 6(a) and 6(b) is in the lack of the peak at

$\omega \sim 2.6\omega_0$ in the case of the t-J Holstein model. To further strengthen our claim, we present optical spectra for various values of magnetic exchange interactions J/t. By increasing J/t magnetic peaks shift toward higher frequencies that should further separate magnetic and lattice degrees of freedom. Nevertheless, we observe no signature of peaks around $\omega \sim 2.6\omega_0$ as they would appear in the corresponding Holstein model. The effect of increasing λ is seen only through widening of magnetic peaks as also observed in Fig. 4. When using much smaller value of the artificial damping ϵ, small peaks, spaced by $\Delta\omega \sim \omega_0$ appear around magnetic peaks.

V. SUMMARY

In summary, we have explored effects of magnetic as well as lattice degrees of freedom on optical properties of the t-J Holstein model. EDLFS captures well optical properties of a single hole in the t-J Holstein model in the range of physically relevant parameters of the model since it treats spin and lattice degrees of freedom on equal footing. Competition between kinetic energy and spin degrees of freedom strongly influences the coherent hole motion as measured by charge stiffness near the crossover to SC polaron regime. In the adiabatic regime increasing EP coupling leads to the shift of the OC spectra toward higher frequencies and broadening of peaks that in the pure t-J model originate in magnetic excitations. As an unusual, however, important finding we report a lack of a peak in the OC spectra at or slightly above the phonon frequency that we attribute to the inherently strong correlations that are present in the t-J model. This finding suggests that within the framework of the t-J Holstein model the two-peak structure seen in recent optical measurements is entirely due to magnetic excitations. Based on our calculations, the two-peak structure can be explained with the observation of local magnetic excitations, created by the hole motion at lower frequencies and the contribution of spin waves, coupled via doped hole to lattice degrees of freedom at higher frequencies.

ACKNOWLEDGMENTS

J.B. acknowledges stimulating discussions with I. Sega, A. S. Mishchenko, and the financial support of the SRA under Grant No. P1-0044. J.B. furthermore acknowledges R. Krivec for his valuable numerical support and maintaining extremely stable operating system on Sun clusters where all numerical calculations have been performed. S.M. acknowledges the financial support of the Next Generation Super Computing Project of Nanoscience Program, CREST, and Grant-in-Aid for Scientific Research from MEXT.

[1] A. Ramšak, P. Horsch, and P. Fulde, Phys. Rev. B **46**, 14305 (1992).
[2] W. Meevasana, *et al.*, Phys. Rev. Lett. **96**, 157003 (2006).
[3] O. Rösch, O. Gunnarsson, X. J. Zhou, T. Yoshida, T. Sasagawa, A. Fujimori, Z. Hussain, Z.-X. Shen, and S. Uchida, Phys. Rev. Lett. **95**, 227002 (2005).
[4] X. J. Zhou, *et al.*, Nature (London) **423**, 398 (2003).
[5] A. Alexandrov and N. F. Mott, Rep. Prog. Phys. **57**, 1197 (1994).
[6] O. Gunnarsson, M. Calandra, and J. E. Han, Rev. Mod. Phys. **75**, 1085 (2003).
[7] T. Tohyama and S. Maekawa, Phys. Rev. B **64**, 212505 (2001).
[8] I. Sega and P. Prelovšek, Phys. Rev. B **42**, 892 (1990).
[9] G. Schubert, G. Wellein, A. Weisse, A. Alvermann, and H. Fehske, Phys. Rev. B **72**, 104304 (2005).
[10] A. Alvermann, D. M. Edwards, and H. Fehske, Phys. Rev. Lett. **98**, 056602 (2007).
[11] B. Bäuml, G. Wellein, and H. Fehske, Phys. Rev. B **58**, 3663 (1998).
[12] A. S. Mishchenko, N. Nagaosa, N. V. Prokofev, A. Sakamoto, and B. V. Svistunov, Phys. Rev. Lett. **91**, 236401 (2003).
[13] A. S. Mishchenko, N. Nagaosa, Z.-X. Shen, G. DeFilippis, V. Cataudella, T. P. Devereaux, C. Bernhard, K. W. Kim, and J. Zaanen, Phys. Rev. Lett. **100**, 166401 (2008).
[14] B. Kyung and S. I. Mukhin, Phys. Rev. B **55**, 3886 (1997).
[15] E. Cappelluti, S. Ciuchi, and S. Fratini, Phys. Rev. B **76**, 125111 (2007).
[16] J. Bonča, S. Maekawa, T. Tohyama, and P. Prelovšek, Phys. Rev. B **77**, 054519 (2008).
[17] J. Bonča, S. Maekawa, and T. Tohyama, Phys. Rev. B **76**, 035121 (2007).
[18] J. Bonča, S. A. Trugman, and I. Batistić, Phys. Rev. B **60**, 1633 (1999).
[19] P. F. Maldague, Phys. Rev. B **16**, 2437 (1977).
[20] B. S. Shastry and B. Sutherland, Phys. Rev. Lett. **65**, 243 (1990).
[21] A. Ramšak and P. Prelovšek, Phys. Rev. B **42**, 10415 (1990).
[22] M. M. Zemljič and P. Prelovšek, Phys. Rev. B **72**, 075108 (2005).
[23] J. I. Igarashi and P. Fulde, Phys. Rev. B **48**, 12713 (1993).
[24] P. Prelovšek, R. Zeyher, and P. Horsch, Phys. Rev. Lett. **96**, 086402 (2006).
[25] String states represent excited states of a particle (hole) in the linear potential created by the overturned spins left in the wake of a mobile hole as it propagates through an ordered Néel background. Since spin fluctuation arising from the off-diagonal part of the exchange interaction keep erasing the trace of overturned spins, string states, in reality, represent only a naive and approximate physical picture of excited states of the hole doped in the antiferromagnetic background. The physical realization of the string picture emerges as scaling of excited state energies with J/t as $\Delta E \sim (J/t)^{\eta}$ where $\eta \sim 2/3$.
[26] D. Poilblanc, T. Ziman, H. J. Schulz, and E. Dagotto, Phys. Rev. B **47**, 14267 (1993).
[27] T. M. Rice and F. C. Zhang, Phys. Rev. B **39**, 815 (1989).
[28] E. Cappelluti, S. Ciuchi, and S. Fratini, Phys. Rev. B **79**, 012502 (2009).